A Single-Point, Multiparameter, Fiber Optic Sensor Based on a Combination of Interferometry and LSPR

Harald Ian Muri, Andon Bano, and Dag Roar Hjelme

***Abstract*—We demonstrate a new single-point, multiparameter, fiber optic sensor concept based on a combination of interferometric and plasmonic sensor modalities on an optical fiber end face. The sensor consists of an extrinsic Fabry–Perot interferometer in the form of a hemispherical stimuli-responsive hydrogel with immobilized gold nanoparticles (GNPs). The GNPs exhibit local surface plasmon resonance (LSPR) that is sensitive toward the local refractive index (RI) of the surrounding environment, whereas the stimuli-responsive hydrogel is sensitive toward specific chemical compounds. We evaluate the quality of the interferometric and LSPR signals as a function of GNP concentration and of hydrogel swelling degree stimulated by ethanol solutions. The GNPs have little influence on the visibility of the Fabry–Perot etalon. The swelling degree of the hydrogel, with corresponding bulk RI changes, has little influence on the local surface RI of the GNPs. We expect this novel sensor concept to be of great value for biosensors for medical applications.**

***Index Terms*—Fiber optic sensors, hydrogel, LSPR, multiparametric sensor, nanoplasmonics, smart hydrogel.**

I. Introduction

THE multiplexing capabilities of optical fiber sensors (OFS) are well known and have been widely commended in the research literature. Multiplexed OFSs offer new sensing capabilities by combining multiple sensing elements, such as fiber Bragg gratings and Fabry-Perot (FP) interferometers, to measure different parameters. While these sensors have multi-parameter capabilities, they are relatively large and can not easily be used to sense multiple parameters in a single spatial point as required in many application. E.g. for medical applications, there is a great need for sensing multiple parameters in one single point, combined with other important features like small dimensions, label-free sensing, real-time monitoring and high sensitivity. By sensing several parameters it is also possible to correlate the relevant parameters to achieve higher accuracy. OFSs can fulfill many of these requirements by exploiting intrinsic or extrinsic light-matter interactions at the core-cladding interface or on the fiber end face.

Localized surface plasmon resonance (LSPR) of noble metal nanoparticles (NMNP) are promising candidates for label-free sensing. The label free sensing can be multi-parametric by spectrally resolving different LSPRs observed for NMNP of different size and shape [1]. Most LSPR based fiber optic sensors proposed over the last decade use noble metal nanostructures interacting with the evanescent field at the fiber core-cladding interface or with the light at the fiber end face [2], [3]. The use of fiber end face offers simpler manufacturing methods as compared to utilizing the evanescent field, since there is no need for cladding removal.

We have earlier demonstrated a proof-of-concept fiber optic LSPR sensor based on reflection from spherical gold nanoparticles (GNP) embedded in a hydrogel on a multi-mode (MM) fiber end face [4]. Immobilizing the GNPs in a 3-dimensional polymer network (hydrogel) have two distinct advantages; (i) it enables immobilization of very large number of particles giving a strong LSPR signal, and (ii) it will reduce negative effects on analyte diffusion and binding to functionalized nanoplasmonic surfaces. In addition, the method for immobilizing GNP in the hydrogels is flexible with the possibility of exchanging the GNPs with other NMNPs to obtain high refractive index (RI) sensitivity and LSPR amplitude [5].

Extrinsic Fabry-Perot interferometers (EFPI) are among the simplest and most utilized fiber optic sensors. They are both easy to manufacture and cost effective for a range of applications [6], [7]. We have earlier developed a flexible EFPI technology platform based on a hemispherical smart hydrogel immobilized on the optical fiber end face [8]. This EFPI may be customized for a range of applications and enables implementation of in vivo sensors with unique advantages in terms of miniaturization and cost effectiveness [9]–[11].

In this paper, we demonstrate a new multi-parameter sensor concept by combining an interferometric and a plasmonic sensor on an optical fiber end face, providing two sensing modalities in one single point. The sensor consists of an EFPI in the form of a semi-spherical hydrogel with immobilized GNPs, as presented in Fig. 1. We combine the LSPR of the GNPs in the visible (VIS) range with the interferometric measurements of the EFPI in the infrared range (IR) using a dual core optical fiber (DCOF). By guiding VIS light in the large core (first cladding) it is possible to achieve a high numerical aperture (NA) for excitation and collection of the LSPR of the GNPs. Accurate interferometric measurement of the hydrogel cavity is made possible by

Manuscript received July 31, 2017; revised October 27, 2017 and December 19, 2017; accepted January 6, 2018. Date of publication January 9, 2018; date of current version February 24, 2018. This work was supported in part by the strategic research fundings from the Norwegian University of Science and Technology (NTNU), in part by the Interreg Sweden-Norway program (IR2015.01), and in part by the Energy and Sensor Systems group (ENERSENSE, strategic research program at NTNU). This paper was presented in part at the 25th International Conference on Optical Fibre Sensors, Jeju, South Korea, April 24–28, 2017. *(Corresponding author: Harald Ian Muri.)*

The authors are with the Department of Electronic Systems, Norwegian University of Science and Technology (NTNU), Trondheim 7491, Norway (e-mail: harald.muri@ntnu.no; andon2105@hotmail.com; dag.hjelme@ntnu.no).

Color versions of one or more of the figures in this paper are available online at http://ieeexplore.ieee.org.

Digital Object Identifier 10.1109/JLT.2018.2791722

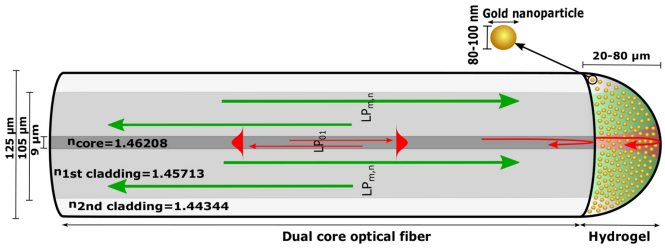

Fig. 1. Illustration of the dual core optical fiber combining interferometric and plasmonic sensor modalities with $n_{\text{core}} = 1.46208$, $n_{\text{1st cladding}} = 1.45713$, and $n_{\text{2nd cladding}} = 1.44344$. IR light is confined as single transverse mode both in the fiber and in the hydrogel volume with reflection at OF-hydrogel interface and hydrogel-solution interface illustrated with red color. MM VIS light is guided in first clad with numerical aperture illustrated with green on fiber end face. The FP interferometer is measured with IR while LSPR from GNP is measured with VIS.

confining the IR light in the core to create single mode (SM) wave propagation. This design avoids the limitations of modal dispersion in MM EFPI in the IR at the same time as we suppress the interference in the VIS range were the fiber is highly MM [12].

Since both the FP resonances and the LSPR are sensitive to changes in the hydrogel RI, the sensor design is susceptible to cross-talk. However, in a sensing configuration where the interferometer is used to sense hydrogel swelling and the plasmon resonance is used to sense binding to receptors immobilized at the GNP surface, we expect the crosstalk to be small. In this situation, the changes in the FP signal caused by the large physical swelling of the hydrogel will dominate over the minute change in bulk RI. Similarly, the change in plasmon resonance will be dominated by analyte binding to surface immobilized receptors rather than the density of the polymer chains.

In this first proof-of-concept demonstration we show that the quality of the interferometric and the LSPR signal are sufficient for dual parameter sensing. The influence of GNPs on the EFPI is investigated by characterizing the visibility and the free spectral range (FSR) of the interferometric signal as a function of increasing GNP density. Similarly, the influence of hydrogel swelling degree on the LSPR signal is investigated by characterizing the LSPR as a function of decreasing optical path length of the hydrogel. Finally, we characterize dried GNP-acrylamide hydrogel and pregel using scanning electron microscope (SEM) to study particle distribution and morphology of the hydrogel.

The detailed performance characterization of the interferometric and the LSPR sensor is beyond the scope of this proof-of-concept demonstration.

II. Sensor Implementation With DCOF

A. Fabry-Perot Interferometer

The stimuli-responsive hydrogel shown in Fig. 1 represents a low-finesse FP etalon. The FP is interrogated using IR light guided by the single-mode core. Confining the IR light to a single transverse mode, both in the fiber and in the hydrogel volume, ensures effective interference between the field reflected at fiber-gel interface and the field reflected at the gel-solution interface (as illustrated with red color in Fig. 1). Both the reflection at the

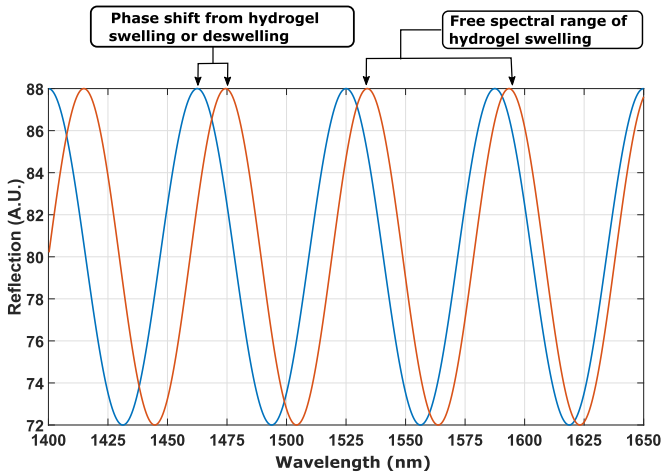

Fig. 2. Illustration of the spectral response by utilizing a stimuli responsive hydrogel as EFPI sensor with optical length ~24 μm. Simulation from FP-etalon equations in Matlab.

gel-solution interface, r_2, and at the fiber-gel interface, r_1, are small, and multiple reflections can be safely neglected. The total IR reflection from the hydrogel FP can therefore be described as the sum of two waves resulting in the intensity,

$$\mathrm{I}(\lambda) = \mathrm{I}_0 \left[{\mathrm{r}_1}^2 + (\gamma \mathrm{r}_2)^2 + 2\gamma \mathrm{r}_1 \mathrm{r}_2 \cos\left(\frac{4\pi l_0}{\lambda} + \varphi_0 \right) \right] \quad (1)$$

where $k = \frac{2\pi}{\lambda}$, l_0 is the optical length of the hydrogel cavity, γ is a loss factor (due to absorption, scattering, and mode mismatch), and φ_0 is an arbitrary phase.

The IR reflectance spectra are characterized by three parameters; visibility, FSR, and phase shift (illustrated in Fig. 2). The visibility can be expressed as,

$$V = \frac{2\gamma \mathrm{r}_1 \mathrm{r}_2}{{\mathrm{r}_1}^2 + (\gamma \mathrm{r}_2)^2} \quad (2)$$

The FSR is the distance between the maxima of $\mathrm{I}(\lambda)$ and can be expressed as,

$$\mathrm{FSR} = \frac{{\lambda_0}^2}{2 l_0} \quad (3)$$

where λ_0 is the center wavelength of the light source. The phase change of the reflectance spectrum is given by the change in optical length as,

$$\Delta\phi = \frac{4\pi \Delta l_0}{\lambda_0} \quad (4)$$

The change in l_0 may originate from both a change in RI of the hydrogel and from a change in the physical length l of hydrogel cavity,

$$\Delta l_0 = \Delta l n_{\text{gel}} + l \Delta n_{\text{gel}} \quad (5)$$

where n_{gel} is the RI of the hydrogel, originating from both the solvent and the polymer concentration.

B. Localized Surface Plasmon Resonance Sensing

The LSPR of the GNPs in the hydrogel is probed using VIS light guided in the MM first cladding as shown in Fig. 1. Using

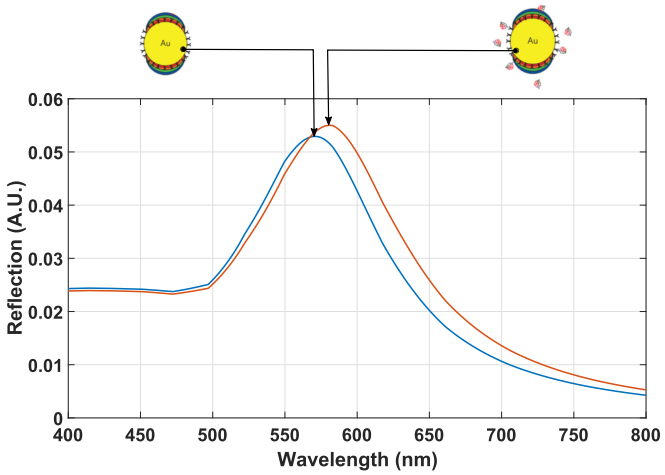

Fig. 3. Illustration of the spectral response of the LSPR sensing with GNPs (80 nm diameter). Simulation from Mie solutions in Matlab.

the high NA of the large diameter core for the VIS light ensures effective excitation of a large fraction of the GNPs immobilized in the hydrogel volume and effective collection of scattering from the LSPR of the GNPs (as illustrated with green color in Fig. 1).

The reflection from GNPs is a result of both scattering and absorption, however, in our case the reflection from the GNP-hydrogel is dominated by scattering. With a sufficient low GNP density, and absence of dipole-dipole interactions, the optical properties of GNPs in hydrogel can be described by Mie theory for spheroidal particles (as used in Fig. 3) or extended by Gans theory for non-spheroidal particles [13], [14].

The scattering cross section is maximized when the real part of the dielectric function of the GNP, $\varepsilon_1(\lambda)$, and the dielectric constant of surrounding medium, $\varepsilon_{\text{local}}$, has the relation [1],

$$\varepsilon_1(\lambda) = -2\varepsilon_{\text{local}} \tag{6}$$

If the dielectric medium around the GNP change, the wavelength of the LSPR change. By using the Drude model, the LSPR peak position as a function of local RI, $n_{\text{local}} = \sqrt{\varepsilon_{\text{local}}}$, within a sufficiently narrow range can be described as,

$$\lambda_{\max} = \lambda_p \sqrt{2{n_{\text{local}}}^2 + 1} \tag{7}$$

where λ_p is the plasma oscillation wavelength of the bulk metal [15]. The change from $\lambda_{\max(1)}$ to $\lambda_{\max(2)}$ with respect to $n_{\text{local}(1)}$ and $n_{\text{local}(2)}$ can be expressed as,

$$\frac{\lambda_{\max(1)}}{\lambda_{\max(2)}} = \sqrt{\frac{2{n_{\text{local}(1)}}^2 + 1}{2{n_{\text{local}(2)}}^2 + 1}} \tag{8}$$

In terms of hydrogel composition and GNP concentration, the two sensing modalities results in conflicting requirements. High visibility of the interference signal can be obtained by using high polymer density hydrogel and low GNP density. High LSPR signal is obtained using a hydrogel with high GNP density. A low polymer density hydrogel is also advantageous for LSPR sensing to reduce the effect of polymer chains in close proximity to the plasmonic wave, as well as to allow analyte diffusion in to the hydrogel volume. The hydrogel composition and GNP density must be tailored to reach the desired interferometric and LSPR sensing requirements as defined by the applications in mind.

III. Materials and Methods

A. Fabricating the GNP-Hydrogel

The fiber optic sensor was fabricated as described in earlier work [4]. 560 nm resonant GNPs in citrate buffer (80 nm diameter, 7.8×10^9 particles/mL, Sodium Citrate 0.1 mg/mL, Sigma-Aldrich, Schnelldorf, Germany) and 575 nm resonant GNPs in citrate buffer (100 nm diameter, 3.8×10^9 particles/mL, Sodium Citrate 0.1 mg/mL, Sigma-Aldrich) were densified to particle density of 1.95×10^{11} and 1.9×10^{11} mL^{-1}, respectively, and used for making pregel solutions containing 10 wt% acrylamide (Sigma Aldrich) and 2 mol% N,N-methylenebisacrylamide (BIS) (Sigma Aldrich).

B. Fabricating GNPs on Bare DCOF End Face

Randomly adsorbed GNPs on bare DCOF end face for the VIS measurements in air were prepared by immersing a bare DCOF in the densified GNP citrate buffer (80 nm, 1.95×10^{11} particles/mL). The bare DCOF was withdrawn out of the GNP citrate buffer solution so a semi-spherical drop covered the OF end face. The OF was then dried for 1 min and subsequently cleaned with 96% ethanol to remove excess GNPs and impurities.

C. Setup of the FO Sensor Instrument

The fiber optic sensor set-up illustrated in Fig. 4 consist of the following components; VIS broadband source (MBB1F1, 470–850 nm, Thorlabs, Stockholm, Sweden), IR broadband source (S5FC1005S, 1550 nm, 50 nm bandwidth, Thorlabs), 50:50 coupler MM (50/50, FCMH2-FC, 400–1600 nm, Thorlabs), 50:50 coupler SM (50/50, 84075633, 1550 nm, Bredengen, Oslo, Norway), double cladded optical fiber coupler (DC1300LEB, MM 400–1700 nm, SM 1250–1550 nm, Thorlabs), VIS spectrometer (QE65Pro, Ocean Optics, Oslo, Norway), IR spectrometer (NIRQuest-512-1.7, Ocean Optics), loose fiber-end terminated with index matching gel (G608N3, Thorlabs), LSPR and FP sensor segment with Ø125 μm DCOF (DCF13, Thorlabs).

The program Spectrasuite (Ocean Optics) was used to obtain the spectra and the optical fibers were spliced using a Fitel Fusion Splicer (Furukawa Electric, Tokyo, Japan).

D. Preparation of Solutions for Hydrogel Swelling and Deswelling

Ethanol (96%, Sigma Aldrich) were added to mQ-water to prepare solutions for hydrogel swelling and deswelling for the IR and VIS measurements of the fabricated GNP-hydrogel.

E. Reflectance Measurements in VIS and IR

The reflectance spectra were estimated from the measured raw spectra S_λ normalized to a measured reference spectra R_λ. Before normalization, we subtracted the measured dark

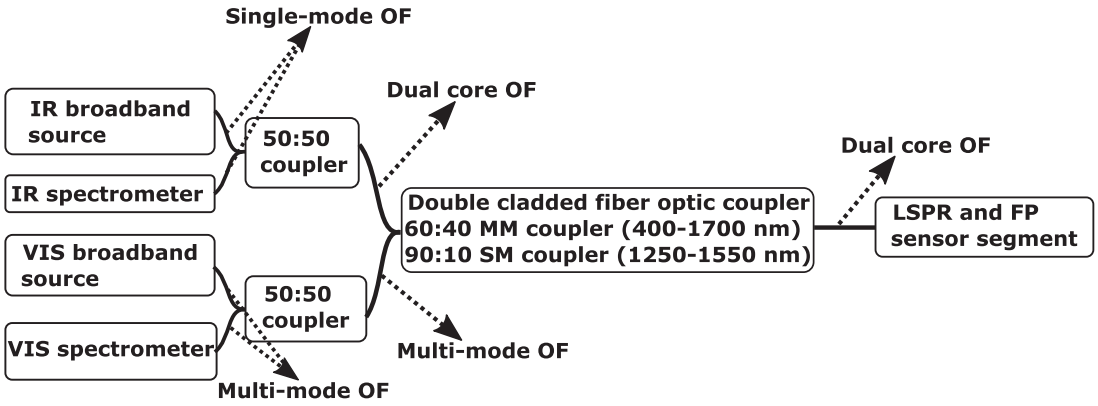

Fig. 4. Set-up of the fiber optic instrument based on reflection measurements.

spectrum D_λ (recorded with the light source turned off) from both the raw spectra and a reference spectra. Thus, the normalized reflectance spectra were computed as,

$$I_{\mathrm{R}} = \left(\frac{S_\lambda - D_\lambda}{R_\lambda - D_\lambda} \right) \times 100\% \tag{9}$$

The hydrogel swelling, or deswelling, was induced by immersing the hydrogel-fiber in solutions with ethanol concentrations between 30 and 45%. For each solution, the hydrogel was left for 1 minute to reach equilibrium before sampling the reflectance spectrum.

It is convenient to use different reference spectra in (9) for the different experiments;

- For all IR experiments we used the raw spectra from the reflections of the bare DCOF in mQ-water solution.
- For the VIS experiments with GNP-hydrogel, we used the raw spectra from the hydrogel without GNP for each ethanol concentration to compensate for the artefacts in the LSPR spectra caused by the hydrogel.
- For the VIS experiments with the sensor in air, we used the raw spectra from the bare DCOF in air.
- For the VIS experiments of hydrogel without GNP in ethanol, we used the raw spectra of the bare DCOF in ethanol.

Scattering increases with increasing GNP size, with an associated spectral broadening of the LSPR signal. We observe strong LSPR signal for GNPs with diameter $\geq$80 nm and particle density $\geq 2 \times 10^{10}$ mL^{-1}. The visibility measurements were obtained with GNP diameter of 100 nm, whereas for the hydrogel swelling measurements the GNP diameter were 80 nm.

F. Estimating the FSR and the LSPR Peak Position

We determined the FSR from the autocorrelation function of the reflectance spectra to relax the dependence on signal normalization. The results demonstrates that both the raw spectra S_λ as well as the normalized reflection spectra I_{R} can be used.

The autocorrelation function is symmetric and measures the correlation between $x_{(i)}$ and $x_{(i+k)}$, with $x = I_{\mathrm{R}}$ or $x = S_\lambda$, for lag time $k = 0, 1, 2...(N-1)$ where N is the length of the vector received from the spectrometer. The autocorrelation coefficients for lag time k is described as,

$$r_k = \frac{\sigma^2}{N-1} \sum_{i=1}^{N-k} (x_{(i)} - \overline{x})(x_{(i+k)} - \overline{x}) \tag{10}$$

where σ^2 is the sample variance of the lag time series and $\overline{x}$ is the mean of x [16]. To find the FSR, the centered and scaled smoothing spline function was applied on the first peak of the autocorrelation function with a smoothing parameter at 0.995. With smoothing parameter $p = 0$ the smoothing spline function produces a least-squares line fit to the data, whereas with $p = 1$ the smoothing spline function produces a cubic spline interpolant. By choosing a fixed smoothing parameter the balance between residual error and local variation is also fixed [17].

For the VIS reflectance measurements of GNPs, the LSPR spectrum was fitted with a centered and scaled smoothing spline function with smoothing parameter at 0.95.

G. Visibility Measurements

The quality of the FP etalons were assessed by the visibility parameter,

$$V = \frac{\max(I_{\mathrm{R}}) - \min(I_{\mathrm{R}})}{\max(I_{\mathrm{R}}) + \min(I_{\mathrm{R}})} \tag{11}$$

All visibility experiments were conducted by having the OF sensor in mQ-water.

H. Characterization With Scanning Electron Microscopy

The acrylamide hydrogel with GNPs were prepared for SEM (Teneo VS, FEI) to preserve their inner morphology. The GNP-acrylamide hydrogel was fabricated as described in previous work [4], with monomers used in this paper in bulk volume of $\approx$0.5 cm^3 and fixated in 2.5% glutaraldehyde (Sigma-Aldrich) for 2 hours at room temperature. The hydrogel in glutaraldehyde was then left for 12 hours at 4 °C and washed two times for 5 minutes in phospate buffered saline (PBS) (Sigma-Aldrich). The hydrogel was further dehydrated with ethanol for 5 minutes at concentration of 10, 25, 50, 70 and 90%, and in the end dehydrated with ethanol two times for 5 minutes at 96 and 100%. After the dehydration, the hydrogel was subsequently transferred to the critical point drier (CPD) (E3000 Series II,

Polaron). With low temperature and high pressure the ethanol was replaced with liquid carbon dioxide and further sublimed entirely. After the CPD the hydrogel sample was cut or cracked in two by a razor, immobilized on carbon tape, and sputter coated (E5100, Polaron) with 40–60 nm of gold to enhance the electron emissivity and conductivity of the sample.

The pregel solution of acrylamide and GNP was also prepared for SEM to characterize the particle distribution. mQ-water was used to dilute the GNP-acrylamide pregel solution to a ratio of 1/1000 (pregel/mQ water). The diluted GNP-acrylamide pregel solution was subsequently transferred onto carbon tape for drying in air at room temperature. The diluted and dried GNP-acrylamide pregel was then sputter coated with 40–60 nm of gold.

IV. Results and Discussion

First, we assessed the quality of the interferometric and plasmonic signals from the hemi-spherical acrylamide hydrogel with immobilized GNPs. Second, the influence of the GNPs on the FP cavity was determined by measuring the visibility and FSR as a function of GNP density. Next, the influence of hydrogel swelling, or deswelling, on n_{local} at the GNP surfaces was determined by measuring the spectral shift of the LSPR peak and FSR as a function of ethanol concentration. Finally, we characterized the particle distribution and the surface morphology of the GNP-acrylamide hydrogel using SEM.

A. Quality of the LSPR and the Interferometric Signals

Fig. 5(a) shows IR reflectance spectra of hydrogels with and without GNP (80 nm, 1×10^{11} particles/mL) in 30% ethanol solution. The resulting autocorrelation function of the reflectance spectrum used to find the FSR is shown in Fig. 5(b).

The visibility is largest for the hydrogel without GNP, while the mean reflectance of hydrogel with GNP is largest. This indicates that the ratio $\frac{\gamma r_2}{r_1}$ is increasing in the presence of GNPs. However, the visibility and the mean reflectance will also vary with the geometries of the manufactured FO sensors. The visibility as a function of GNP density is characterized in Section IV-B to evaluate the quality of the FP cavity and to investigate the influence of GNP on the interference.

The VIS spectrum in Fig. 6(a) shows the reflectance of GNP-hydrogel (80 nm, 1×10^{11} particles/mL) in 30% ethanol solution. The LSPR signal is a 7% resonance peak (measured from first minimum and first maximum) on top of a 90% background reflectance. It follows from Fig. 6(b) that this background reflectance is mainly due to the Fresnel reflection at the fiber-gel interface. The level of background reflectance will also vary with the composition of the hydrogel. As expected we observe no interference fringes since the MM propagation in fiber and hydrogel washes out the interference. The resonance can however be improved by increasing the particle density.

For comparison we have also included VIS reflectance measurements of randomly adsorbed the GNP on bare DCOF end face in air in Fig. 6(a). The strength of the LSPR signal is a -2% resonance peak. The negative LSPR amplitude represents an absorption of the close-packing of GNPs that is comparable

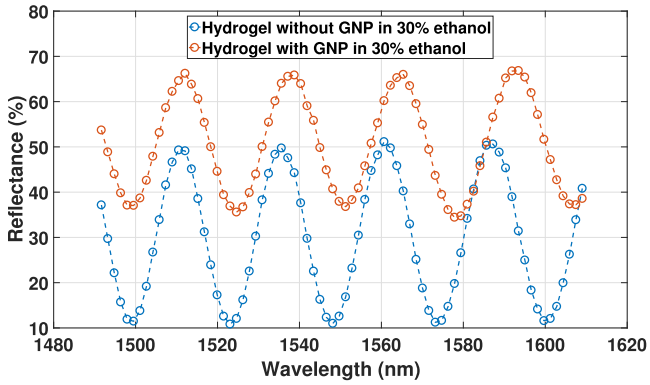

(a)

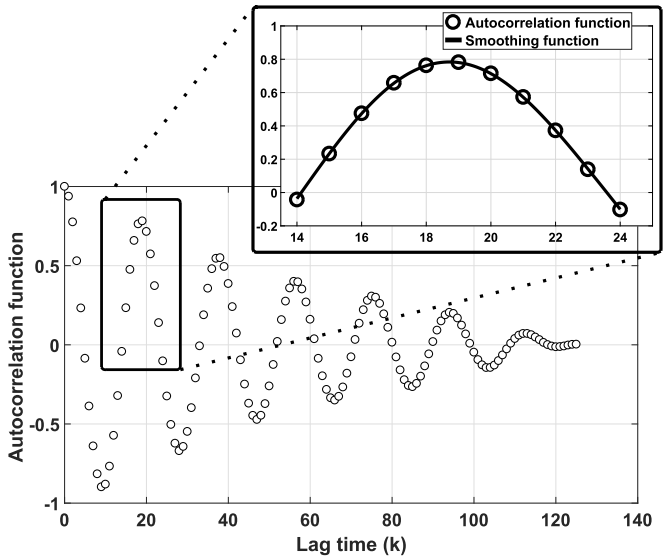

(b)

Fig. 5. (a) IR reflectance from the hydrogel with and without GNPs (80 nm, 1×10^{11} particles/mL) on fiber end face in 30% ethanol; (b) Autocorrelation function of the reflectance spectrum from GNP-hydrogel in Fig. 5(a).

to results from previous work [18]. We note that this is also different from other work, e.g., from the fabrication of periodic noble metal nanostructures on OF end face [2].

The LSPR for GNP on bare DCOF end face is at 566 nm compared to 572 nm for the GNP-hydrogel. The difference is due to the different fabrication methods used and due to the different surrounding RIs. The LSPR for GNP-hydrogel also differs from the LSPR at 560 nm for GNP citrate buffer solution. The redshift is due to the n_{gel} from the ethanol solution and the polymer network, compared to the RI of the citrate buffered solution. The change in local RI can be computed from (8). With RI of GNP-citrate solution as $n_{\mathrm{local}(1)} = 1.33$ [19], $\lambda_{\mathrm{max}(1)} = 560$ nm, and $\lambda_{\mathrm{max}(2)} = 572$ nm, the local RI will be $n_{\mathrm{local}(2)} = 1.3665$. The computed local RI $n_{\mathrm{local}(2)} = 1.3665$ is close to the RI of 30% ethanol at 1.3535 [19].

B. Visibility and FSR as a Function of GNP Density

Fig. 7 shows the visibility and the FSR of the hydrogel cavity for increasing density of 100 nm GNPs. No distinct decrease

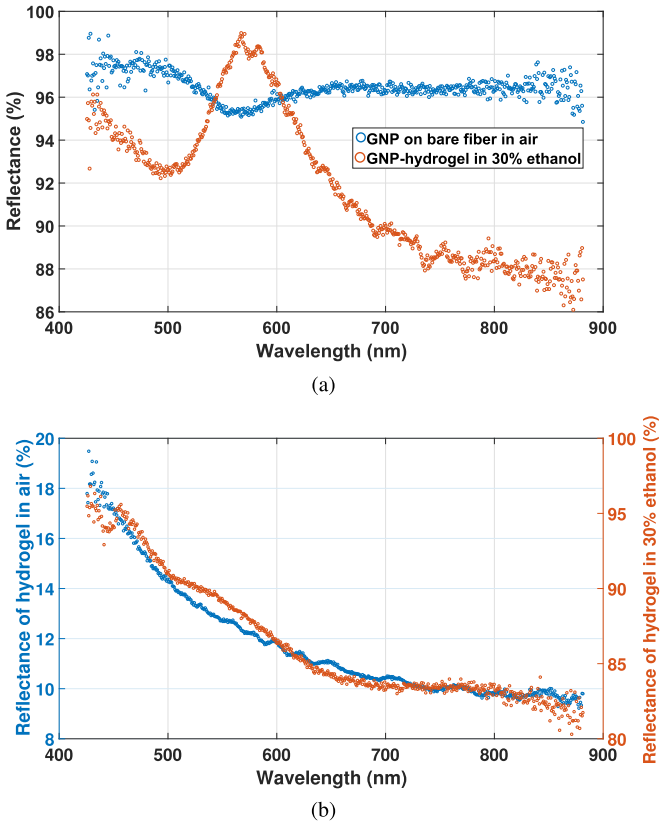

Fig. 6. (a) VIS reflectance of GNP on fiber end face in air and of GNP-hydrogel (80 nm, 1×10^{11} particles/mL) on fiber end face in 30% ethanol solution; (b) VIS reflectance of hydrogel without GNP on fiber end face in air and in 30% ethanol solution.

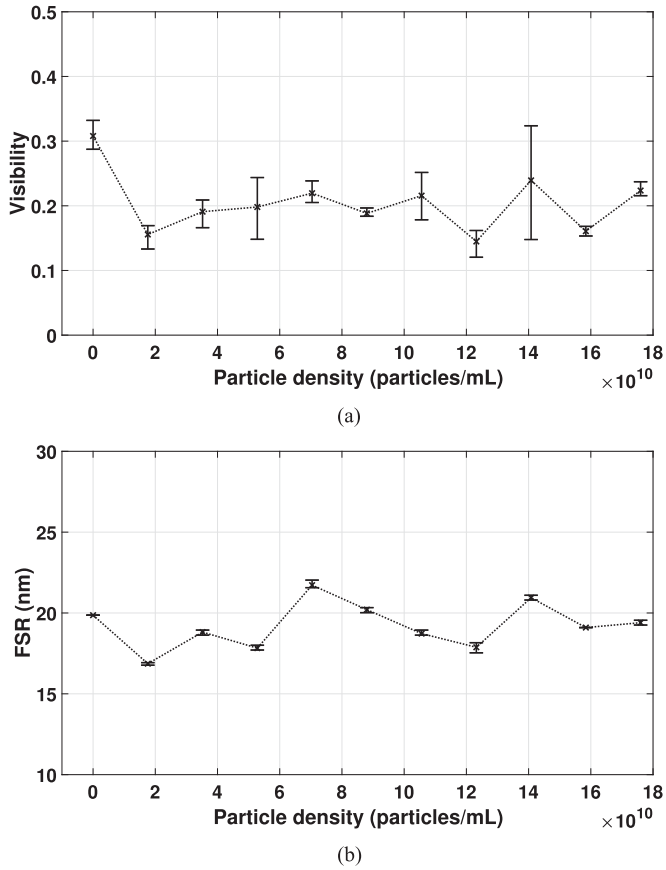

Fig. 7. (a) Visibility measurements of hydrogel for increasing particle density (100 nm diameter); (b) FSR of hydrogel as a function of particle density. Each data point represents the mean, with error bars showing the maximum and minimum values of the estimated visibilities and FSRs based on 5 sampled spectra.

in visibility with increasing particle density is observed. The mean visibility fluctuates between 0.17 and 0.3 (not including the measurements without GNPs), a variation most likely due to variations of the geometry of the different manufactured FO sensors. The initial drop in visibility after adding GNPs to the hydrogel might be due to GNPs adsorbing to the surfaces. With no distinct decrease in visibility for increasing GNP density, we conclude that the quality of the FP interferometer is not limited by the amount of GNPs immobilized in the hydrogels in our experiments. The visibility is comparable to previous work on EFPI [9] and the sensitivity would therefore be similar.

The FSR is fluctuating between 18 nm and 22 nm with GNP density in Fig. 7(b). Small variations in FSR are expected to occur for the different sensors due to the variation in pregel droplet size deposited on the fiber end face. A variation between 5 to 10 μm for the different manufactured sensors is likely to occur and would change the FSR with 2 to 4 nm comparable to the variance observed in Fig. 7(b). The dependence or independence of FSR on GNP density is therefore uncertain. The change in optical length for the change in n_{gel} in (5) should be negligibly small when adding GNPs to the hydrogel. However, the polymerization process could be influenced by the GNP citrate buffer solution in the pregel and change the physical length l in (5). It is important to note that the variation in the FSR with GNP density is not important for a sensor application, since it is the *change* in FSR that contains information about the measurand.

C. FSR and LSPR as a Function of GNP-Hydrogel Swelling and Deswelling

Fig. 8(a) shows the measured FSR for the deswelling GNP-hydrogel with particle density at 1×10^{11} and 5×10^{10} mL^{-1} controlled with increasing ethanol concentrations. The FSR follows the same trend for the two particle densities for ethanol concentrations from 30% to 45%. The FSR increases monotonically from 25 nm to 45 nm and from 30 nm to 55 nm for particle density at 1×10^{11} and 5×10^{10} mL^{-1}, respectively. The difference between the FSR for particle density at 1×10^{11} and 5×10^{10} mL^{-1} can not be concluded to be dependent or independent on GNP density due to the variance in FSR as a result of the sensor preparations as discussed in Section IV-B. Despite having GNPs immobilized in the hydrogel, the readout of the FSR give accurate information of the swelling dynamics of stimuli-responsive hydrogels. This is also evident from the visibility measurements from Fig. 7(a) that is comparable to previous work on EFPI [9]. The sensitivity would therefore be similar to earlier results and sufficient for many applications. Using phase detection algorithm would further improve the sensitivity compared to the FSR measurements used in this work [9].

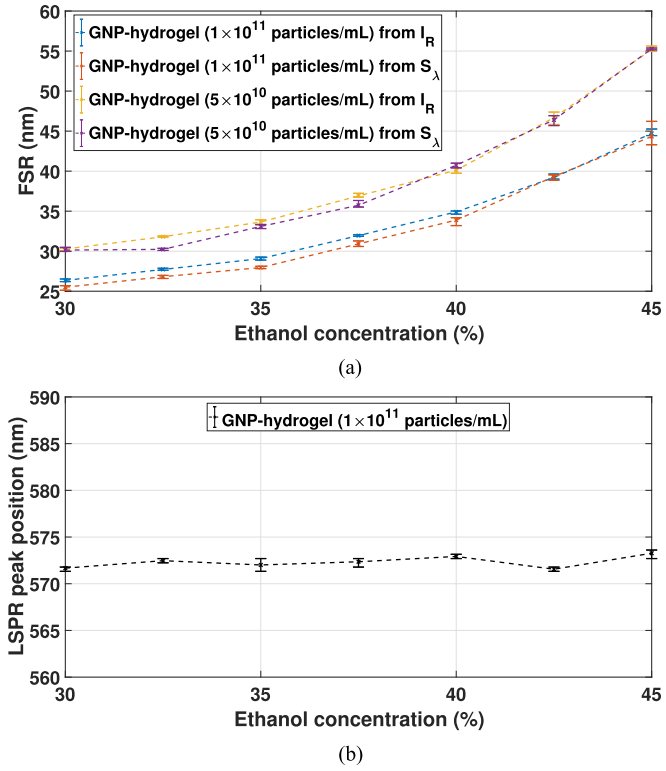

Fig. 8. (a) FSR from reflectance I_{R} and raw S_λ spectra measured for decreasing hydrogel size controlled with ethanol solutions; (b) LSPR peak with corresponding wavelength measured for decreasing hydrogel size controlled with ethanol solutions. Each data point represents the mean, with error bars showing the maximum and minimum values of the estimated FSR and LSPR based on 4 sampled series of the spectra for the increase and decrease in ethanol concentration.

The nonlinear response of FSR in Fig. 8(a) for increasing ethanol concentration occurs as a result of approaching the critical point for dehydration that results in a collapse of the hydrogel when increasing the ethanol concentration beyond 45–50% [20]. The hydrogel contraction rate will therefore increase with increasing ethanol concentration up to the critical point for collapse.

The FSR computed from the raw spectra S_λ have a monotonic response towards increasing ethanol concentration similar to the FSR computed from the normalized reflection spectra I_{R} with a bias or error of 0.9–1.9 nm in Fig. 8(a). Thus, depending on the accuracy required, it might be sufficient to compute the FSR from reflection spectra such as S_λ having a non-ideal interference signal, thereby simplifying the signal processing.

In Fig. 8(b) the LSPR peak position is measured as a function of hydrogel deswelling. The LSPR peak positions are fluctuating between 571.36 nm and 573.64 nm. The hydrogel contraction leads to an increase in the RI of the hydrogel due to the increasing density of acrylamide polymer. A change in ethanol concentration from 30% to 45% results in a solvent RI change of $\Delta\mathrm{RI} = 0.0066$ [19]. The change in n_{gel} as a result of the increase in ethanol concentration as well as a result of the increase in polymer density should result in a redshift. From (8), it follows that the observed $\Delta\lambda_{\mathrm{LSPR}} \approx$2–3 nm corresponds to $\Delta n_{\mathrm{local}} = 0.009$. Thus, $\Delta n_{\mathrm{local}}$ is close to the $\Delta\mathrm{RI}$ for the change in ethanol concentrations alone. The increase in polymer density by a factor of $\gtrapprox 2$ (change in optical length from 50 μm to 25 μm) will also result in a significantly larger increase in n_{gel}. This demonstrates that the increase in n_{gel} is not increasing n_{local} on the GNP, but rather introducing small variations in the local dielectric environment. The reason for this weak dependence is the combination of low polymer concentration and the small refractive index "probes" (80 nm GNPs).

The results found from LSPR and visibility measurements proves the utility of immobilizing GNP in hydrogels to measure both interferometric and LSPR signal with acceptable levels of cross-talk to obtain label free and selective sensing of specific biomolecules for medical purpose [2], [10]. That the significant increase in n_{gel} results in such a small LSPR shift supports the claim of improved nanoplasmonic sensing by immobilizing GNP in a 3-dimensional polymer network.

D. Particle Distribution and Morphology of GNP-Acryalmide Hydrogel

The SEM images of the fractured piece of dehydrated and dried GNP-acrylamide hydrogel are shown in Fig. 9(a) and (b), while the SEM images of diluted and dried GNP-acrylamide pregel is shown in Fig. 9(c).

The pores are clearly visible in Fig. 9(a) and (b), with size ranging from 0.5 to 3 μm. These pores will however change in size for a hydrated hydrogel, since the dehydration is making the hydrogel smaller in volume. Parts of the hydrogel have also collapsed where the pores are absent.

Hydrogels will hydrate its surface after dehydration due to the humidity at room temperature. Despite exposing the hydrogel to a gradient of ethanol concentrations, small pockets of water can be immobilized inside it. The collapsed areas where the pores are absent can therefore be assumed to be a result of insufficient dehydration since liquid carbon dioxide only will exchange efficiently with ethanol in the critical point drying technique. Other morphological characterizations methods such as cryogenic or environmental SEM have been used to characterize hydrogel with a swelling degree closer to its original hydrated state while omitting the fixation, dehydration, and the critical point drying technique [21], [22].

The particle distribution from the SEM image in Fig. 9(b) is difficult to distinguish from artifacts associated to the sample preparations [23]. GNP in biological, or gel-like samples, have been observed with back scattered electrons for samples without metal coating, but with highly conductive sample holders [24]. However, the particle distribution can be characterized by comparing the diluted GNP-acrylamide pregel in Fig. 9(c) with the fractured piece of GNP-acrylamide hydrogel in Fig. 9(b). From Fig. 9(c) the GNP shows to have a single and clustered distribution.

The visibility results in Section IV-B is not distinctively decreasing for increasing GNP density which indicates a dispersed distribution of GNP throughout the hydrogel. The clustering of GNP observed in Fig. 9(c) is then most likely a result of the drying process of the diluted and dried GNP-acrylamide pregel.

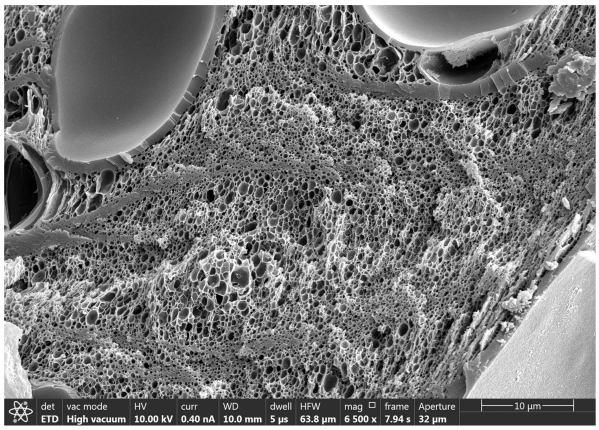

(a)

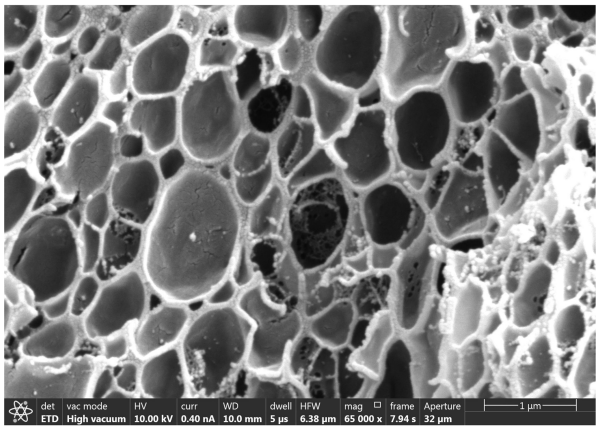

(b)

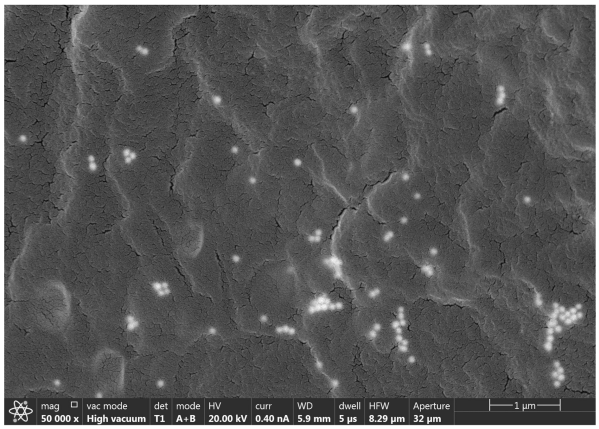

(c)

Fig. 9. (a) SEM image of fractured GNP-acrylamide hydrogel under magnification 10 μm and (b) 1 μm; (c) SEM image of diluted GNP-acrylamide pregel under magnification 1 μm.

V. Conclusion

We have demonstrated a new multi-parameter sensor concept by combining an interferometric and a plasmonic sensor on an optical fiber end face, proving the feasibility of utilizing two label free sensing techniques in one single point. The FO sensor consist of an EFPI in the form of a hemi-spherical hydrogel with immobilized GNPs. The quality of the interferometric GNP-hydrogel cavity was assessed by measuring the visibility as function of GNP densities. Despite having GNPs immobilized in the hydrogel, the visibility remains almost constant with small fluctuations between 0.17–0.3, for the increasing GNP density.

Further, the FSR of the FP interferometer was measured for decreasing hydrogel size, stimulated with increasing ethanol concentrations, to assess the swelling mechanism with GNP immobilized in the acrylamide based polymer network. The FSR was increasing monotonically with hydrogel dewelling, demonstrating the feasibility of utilizing stimuli-responsive hydrogels containing GNP for label free sensing. The visibility is comparable to previous work on EFPI [9] and the sensitivity should therefore be similar to earlier results and sufficient for many applications. Using phase detection algorithm would further improve the sensitivity compared to the FSR measurements used in this work [9].

The LSPR peak position was varying between 571.36 nm and 573.64 nm for increasing ethanol concentrations, proving that the increase in hydrogel deswelling (by a factor of $\gtrapprox 2$) is not significantly increasing n_{local}, but rather introducing small variations in the local dielectric environment. We observe no interference fringes in the VIS spectral range due to the washed out interference of the MM propagation. The quality of the LSPR signal is therefore comparable to other fiber end face based LSPR sensors, e.g., from [25].

In conclusion, the proof-of-concept experiments proves the utility of immobilizing GNP in hydrogel to measure both interferometric and LSPR signal with acceptable levels of cross-talk to obtain label free and selective sensing of specific biomolecules for medical purpose.

Further work will consist of realizing this FO system as a biosensor towards medical applications where specific markers will be detected [2], [10], [11], [25]. Moreover, the concept of combining interferometric and LSPR measurements will be explored in other FO sensor designs. The potential of sensing n_{local} with GNP in the hydrogel with less influence of the n_{gel} will also be investigated with respect to label free and selective multi-parameter sensing.

Acknowledgment

The electron microscopy work was performed at the Cellular and Molecular Imaging Core Facility (CMIC) at NTNU.

References

[1] K. M. Mayer and J. H. Hafner, "Localized surface plasmon resonance sensors," *Chem. Rev.*, vol. 111, no. 6, pp. 3828–3857, Jun. 2011. [Online]. Available: http://dx.doi.org/10.1021/cr100313v

[2] M. Sanders, Y. Lin, J. Wei, T. Bono, and R. G. Lindquist, "An enhanced {LSPR} fiber-optic nanoprobe for ultrasensitive detection of protein biomarkers," *Biosensors Bioelectron.*, vol. 61, pp. 95–101, 2014. [Online]. Available: http://www.sciencedirect.com/science/article/pii/S0956566314003418

[3] S. K. Srivastava, V. Arora, S. Sapra, and B. D. Gupta, "Localized surface plasmon resonance-based fiber optic u-shaped biosensor for the detection of blood glucose," *Plasmonics*, vol. 7, no. 2, pp. 261–268, 2011. [Online]. Available: http://dx.doi.org/10.1007/s11468-011-9302-8

[4] H. I. D. I. Muri and D. R. Hjelme, "Novel localized surface plasmon resonance based optical fiber sensor," *SPIE*, vol. 9702, pp. 97 020L–97 020L–8, 2016. [Online]. Available: http://dx.doi.org/10.1117/12.2212652

[5] H. I. D. I. Muri, A. Bano, and D. R. Hjelme, "Interferometric and localized surface plasmon based fiber optic sensor," *SPIE*, vol. 10058, pp. 10 058–10 058–10, 2017. [Online]. Available: http://dx.doi.org/10.1117/12.2250743

[6] Y.-J. Rao, "Recent progress in fiber-optic extrinsic Fabry-Perot interferometric sensors," *Opt. Fiber Technol.*, vol. 12, no. 3, pp. 227–237, Jul. 2006. [Online]. Available: http://www.sciencedirect.com/science/article/pii/S1068520006000174

[7] H. F. Taylor, "Fiber optic sensors based upon the Fabry-Perot interferometer," *Opt. Eng.*, vol. 76. New York, NY, USA: Marcel Dekker, 2002, pp. 41–74.

[8] D. R. Hjelme, A. Berg, R. Ellingsen, B. Falch, A. Bjørkøy, and D. Østling, "Optical sensing of measurands," U.S. Patent 7 440 110, Oct. 21, 2008.

[9] S. Tierney, D. R. Hjelme, and B. T. Stokke, "Determination of swelling of responsive gels with nanometer resolution. fiber-optic based platform for hydrogels as signal transducers," *Anal. Chem.*, vol. 80, no. 13, pp. 5086–5093, Jul. 2008. [Online]. Available: http://dx.doi.org/10.1021/ac800292k

[10] S. Tierney, B. M. H. Falch, D. R. Hjelme, and B. T. Stokke, "Determination of glucose levels using a functionalized hydrogel optical fiber biosensor: Toward continuous monitoring of blood glucose in vivo," *Anal. Chem.*, vol. 81, no. 9, pp. 3630–3636, May 2009. [Online]. Available: http://dx.doi.org/10.1021/ac900019k

[11] D. R. Hjelme, O. Aune, B. Falch, D. Østling, and R. Ellingsen, "Fiber-optic biosensor technology for rapid, accurate and specific detection of enzymes," in *Proc. Adv. Photon. OSA Tech. Dig.*, 2014, Paper. JTu6A.3. [Online]. Available: http://www.osapublishing.org/abstract.cfm?URI=Sensors-2014-JTu6A.3

[12] X. Wu and O. Solgaard, "Short-cavity multimode fiber-tip Fabry-Pérot sensors," *Opt. Express*, vol. 21, no. 12, pp. 14 487–14 499, Jun 2013. [Online]. Available: http://www.opticsexpress.org/abstract.cfm?URI=oe-21-12-14487

[13] G. Mie, "Beiträge zur optik trüberber medien, speziell kolloidaler metallösungen," *Ann. Physik*, vol. 330, no. 3, pp. 377–442, 1908.

[14] R. Gans, "The form of ultramicroscopic gold particles," *Annalen der Physik*, vol. 37, pp. 881–900, 1912.

[15] T. R. Jensen, M. L. Duval, K. L. Kelly, A. A. Lazarides, G. C. Schatz, and R. P. Van Duyne, "Nanosphere lithography: Effect of the external dielectric medium on the surface plasmon resonance spectrum of a periodic array of silver nanoparticles," *J. Phys. Chem. B*, vol. 103, no. 45, pp. 9846–9853, Nov. 1999. [Online]. Available: http://dx.doi.org/10.1021/jp9926802

[16] G. E. Box, G. M. Jenkins, G. C. Reinsel, and G. M. Ljung, *Time Series Analysis: Forecasting and Control*. Hoboken, NJ, USA: Wiley, 2015.

[17] B. W. Silverman, "Some aspects of the spline smoothing approach to non-parametric regression curve fitting," *J. Roy. Statist. Soc. Series B (Methodological)*, vol. 47, no. 1, pp. 1–52, 1985. [Online]. Available: http://www.jstor.org/stable/2345542

[18] P. M. P. Gouvêa, H. Jang, I. C. S. Carvalho, M. Cremona, A. M. B. Braga, and M. Fokine, "Internal specular reflection from nanoparticle layers on the end face of optical fibers," *J. Appl. Phys.*, vol. 109, no. 10, 2011, Art. no. 103114. [Online]. Available: https://doi.org/10.1063/1.3583582

[19] W. M. Haynes, *Handbook of Chemistry and Physics*, 97th ed., W. M. Haynes, Ed. Boca Raton, FL, USA: CRC, 2016-2017.

[20] K. Bouchal, Z. Sedláková, and M. Ilavský, "Phase transition in swollen gels," *Polymer Bull.*, vol. 32, no. 3, pp. 331–338, Mar. 1994. [Online]. Available: https://doi.org/10.1007/BF00308545

[21] J. Zhang and N. A. Peppas, "Morphology of poly(methacrylic acid)/poly(n-isopropyl acrylamide) interpenetrating polymeric networks," *J. Biomater. Sci., Polymer Ed.*, vol. 13, no. 5, pp. 511–525, Jan. 2002. [Online]. Available: http://dx.doi.org/10.1163/15685620260178373

[22] F. M. Plieva, M. Karlsson, M.-R. Aguilar, D. Gomez, S. Mikhalovsky, and I. Y. Galaev, "Pore structure in supermacroporous polyacrylamide based cryogels," *Soft Matter*, vol. 1, no. 4, pp. 303–309, 2005. [Online]. Available: http://dx.doi.org/10.1039/B510010K

[23] A. Mehdizadeh Kashi *et al.*, "How to prepare biological samples and live tissues for scanning electron microscopy (SEM)," *Galen Med. J.*, vol. 3, no. 2, pp. 63–80, Jun. 2014. [Online]. Available: http://www.gmj.ir/index.php/gmj/article/view/267/123

[24] A. Goldstein, Y. Soroka, M. Frušić-Zlotkin, I. Popov, and R. Kohen, "High resolution SEM imaging of gold nanoparticles in cells and tissues," *J. Microscopy*, vol. 256, no. 3, pp. 237–247, 2014. [Online]. Available: http://dx.doi.org/10.1111/jmi.12179

[25] H.-H. Jeong, N. Erdene, J.-H. Park, D.-H. Jeong, H.-Y. Lee, and S.-K. Lee, "Real-time label-free immunoassay of interferon-gamma and prostate-specific antigen using a fiber-optic localized surface plasmon resonance sensor," *Biosensors Bioelectron.*, vol. 39, no. 1, pp. 346–351, Jan. 2013. [Online]. Available: http://www.sciencedirect.com/science/article/pii/S0956566312005337

Authors' biographies not available at the time of publication.